Available online at www.sciencedirect.com

ScienceDirect

Procedia CIRP 00 (2023) 000–000

www.elsevier.com/locate/procedia

56th CIRP Conference on Manufacturing Systems, CIRP CMS '23, South Africa

Defect detection for large-series automated fibre placement using a neural network-assisted machine vision approach

Alexander Peitz[a]*, Michael Emonts[a], Kai Fischer[a], Christian Brecher[b]

[a]*Aachen Center for integrative lightweight Production AZL RWTH Aachen, Campus Boulevard 30, 52074 Aachen, Germany*

[b]*Werkzeugmaschinenlabor WZL der RWTH Aachen, Steinbachstraße 19, 52074 Aachen, Germany*

* Corresponding author. *E-mail address:* alexander.peitz@azl.rwth-aachen.de

Abstract

Tailored reinforcement structures from carbon fibre-reinforced thermoplastics show high potential for minimizing material volume, wall thickness and overall lightweight potential in plastic parts. Integrating small amounts of carbon fibre unidirectional tape material in injection-molded parts has the ability to maximize lightweight potential. Through a novel manufacturing approach developed by AZL, automated fibre placement becomes viable in large-series manufacturing by reducing cycle times down to 5 seconds. Therefore reliable, defect-free manufacturing becomes vital for economic competitivity. In this paper, a novel approach for defect detection using computer vision in combination with neural networks is developed and analysed for applicability in large-series manufacturing. Different occurring defects during processing are detected and classified. Subsequently, classification accuracy is analysed in regard to the predefined defect classes.

© 2023 The Authors. Published by Elsevier Ltd.
This is an open access article under the CC BY-NC-ND license (https://creativecommons.org/licenses/by-nc-nd/4.0)
Peer-review under responsibility of the scientific committee of the 56th CIRP Conference on Manufacturing Systems

Keywords: Fibre-reinforced plastics, automated fibre placement, machine vision, neural networks, defect detection

1. Introduction

Continuously increasing requirements to reduce carbon emissions as well as plastic waste pushes for new solutions in the field of lightweight materials. Fibre-reinforced plastics (FRPs) have high potential for reducing emissions and substituting both regular plastics and metal parts in chosen applications. These materials possess high specific stiffness- and strength-to-weight ratios, making them ideal for reducing weight in selected applications. However, the integration of FRPs can be used to reduce wall thicknesses, eliminate stiffening ribs and in general reduce the amount of plastic material used.

Through the usage of highly productive manufacturing processes such as the laser-assisted automated fibre placement (LAFP), integrating FRPs into low-to mid-range automobiles, consumer goods and electronics becomes feasible. Through a novel production system development by AZL, manufacturing unidirectional (UD), highly load-optimized and near net-shaped tailored blanks from thermoplastic composites becomes feasible in high production volumes exceeding 10 million parts per year.

LAFP is a complex process with a multitude of different process parameters and influences. As such, the process is prone to defects occurring during manufacturing [1]. In past years, multiple inspection techniques have emerged to inspect manufactured laminates. However, most of these methods are time-consuming, costly and not capable of inline inspection [2]. Standard industrial practice still relies heavily on manual inspection, taking up a considerable amount of total

2212-8271 © 2023 The Authors. Published by Elsevier Ltd.
This is an open access article under the CC BY-NC-ND license (https://creativecommons.org/licenses/by-nc-nd/4.0)
Peer-review under responsibility of the scientific committee of the 56th CIRP Conference on Manufacturing Systems

manufacturing time [1]. This work focuses on an inline-capable, cost-efficient inspection method using computer vision and neural networks. A standard industrial camera is used to inspect the laminate's surface after each placement. The fragmented images are then analyzed by the neural network to detect predefined classes of defects that are commonly occurring during manufacturing. Following up, this information can either be relayed to the operator or quantified by methods of computer vision.

Nomenclature

(C/G)FRP	(Carbon/Glass) fibre-reinforced plastic
LAFP	Laser-assisted automated fibre placement
UD	Unidirectional
CNN	Convolutional Neural Network

2. Related work

Multiple research activities have focused on the influence of manufacturing defects during LAFP on key part characteristics such as stiffness, strength, buckling load and in general mechanical performance [3–7].

In automated fibre placement, different approaches and implementations of inline-capable defect detection systems have been investigated. This work focuses on optical defect detection on the surface of laminates. Semi-automated solutions projecting laser lines on the surface of LAFP parts visually indicate defects to the operator [8, 9].

Cemenska et al. show a fully automated defect detection system based on laser profilometry and feature recognition based on gradient detection [10]. Schuster et al. develop a similar approach based on laser profilometry, leaving open the future employment of machine learning models [11].

Sacco et al. implement detailed work on an automated defect detection system equally based on laser profilometry. Here, methods of feature recognition based on deep learning, through the use of CNNs, notably a ResNet network are shown to be feasible [12–14].

Machine learning methods, especially those based on deep learning are gaining in popularity for composite defect detection. Various defect detection algorithms based on thermographic images [15–17] show good results in composite manufacturing. A novel approach by Yoon et al. uses solitary wave detection in combination with CNNs [18].

Through the combination of geometrical defect description and a classification method based on deep learning approaches, *Tang et al.* develop a viable inspection system for thermoset AFP defects. This semantic segmentation leads to a multi-step detection algorithm with increased performance compared to a previously developed single-stage method [19, 20].

An inspection system using an industrial CCD camera is demonstrated by Tao et al. for the detection of gaps in LAFP [21]. Brysch et al. improve on detection using cameras by integrating a SiamMask artificial neural network and compare this approach to classical edge detection methods [22]. *Zhang et al.* similarly use images acquired from industrial cameras and develop a multi-scale LAFP defect detection algorithm based on CNNs [23].

Meister et al. heavily investigate CNN-supported defect detection methods. Most of the work is based on laser profilometry sensor data as well as artificially generated training data. The authors show that this detection approach is a feasible solution for industrial use-cases [24–29].

It is apparent that defect detection in LAFP is gaining in importance recently. Current solutions in research and industry focus on laser profilometry. With the aim of integrating quality control in large-series manufacturing with scalable machine systems, a cost-effective and reliable solution has to be developed. Therefore, the authors investigate the use of economic 2D camera systems enhanced by machine learning algorithms.

3. Materials and experimental setup

3.1. Machine system

For all trials, the custom designed and developed LAFP machine from AZL, the Ultra-Fast Consolidator, is used, see Figure 1. This machine system has an innovative manufacturing principle, where laminates are built up on individual, flat, low-cost and mobile workpiece carriers acting as tooling. The tooling is a round aluminum plate with a thickness of 10 mm. [30]

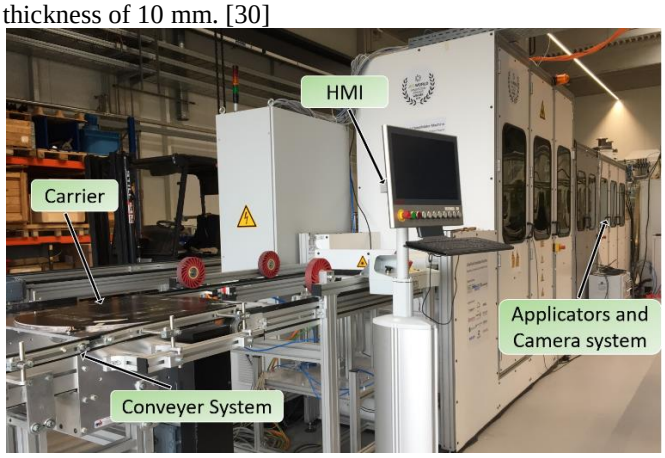


Fig. 1. Ultra-Fast Consolidator machine

Narrow tape placement heads are used to place down the UD tapes onto the carriers. Due to their low width, these placement heads can be easily parallelized and as such, individual laminate layers can be placed down at once, maximizing deposition rate. The used placement head is equipped with an NC axis for automated repositioning and an LDM2500 direct diode laser from *Laserline GmbH*, Germany, with a wavelength of 980 nm and a maximum power output of 2,5 kW. The consolidation roller has a diameter of 60 mm and a shore 45A hardness.

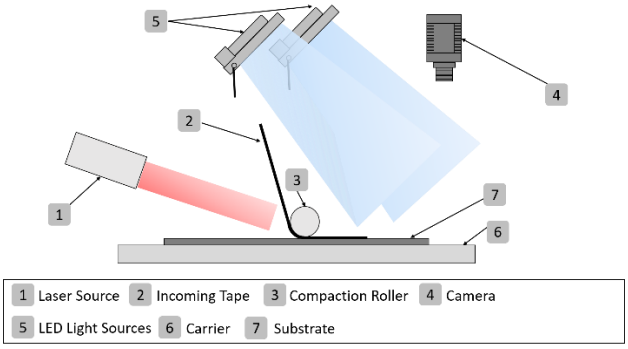


Fig. 2. Measurement setup for defect detection

3.2. Materials

For all trials, polypropylene-CF UD slit tape (width 25 mm, thickness 0,16 mm) was used. As first layer fixation, temperature-resistant double-sided adhesive tape was used.

3.3. Measurement setup

For all trials, an industrial camera DMK 33GP2000e from *The Imaging Source GmbH, Germany*, is used. The camera is equipped with a Ricoh FL-CC2514A-2M manually controlled lens. Two white LED light sources are mounted left and right of the camera to realize optimal lighting conditions (Fig. 2).

The camera is mounted onto the machine frame behind the tape placement head. Due to occurring vibrations during placement, the camera is mechanically decoupled from the head. All samples are taken at a process speed of 100 mm/s.

4. Methodology

4.1. Defect selection

First, a selection of occurring defects in LAFP and especially in the Ultra-Fast machine system is defined. The selection is based on extensive material trials with manual defect determination and quantification. The defects are:

- Gaps > 1 mm
- Overlaps > 1 mm
- Angle deviations > 2°
- Loose tape
- Tape rip
- Thermal surface degradation
- Tape length deviations > 5 mm

4.2. Dataset design and preparation

The camera's video output is transformed directly into individual frames and overlapping images are deleted to eliminate redundancies. The remaining images are then pre-processed in three steps. First, frames containing background noise or undesired components are deleted. Secondly, all images are resized according to the neural net's requirements. All images must be rectangular in size. In this work, two image sizes are used: **450 px * 450 px** and **224 px * 224 px**.

The two image sizes are expected to yield different results. On the one hand, the larger image size contains more information and defects might be sharper to detect. However, it also introduces more redundancy. Finally, all images are sorted into dedicated folders and individually labeled depending on their defect. Fig. 3 shows an example of defect images used to train the neural networks.

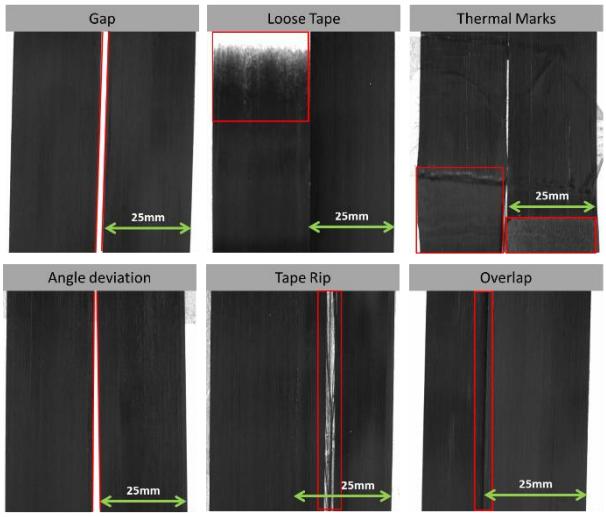


Fig. 3. Exemplary defect images of the considered defect types. Red areas show defects but are not used for training.

4.3. Defect detection and classification

Defect detection is done using different CNNs. First, a general CNN trained on the collected dataset is employed. The CNN's architecture can be taken from Fig. 4. Second, transfer learning with pre-trained CNNs is employed. The used networks are a Visual Geometry Group 16 (VGG16) network and a Residual Neural Network 50 (ResNet50). These two networks are pre-trained on the extremely large ImageNet dataset and are known to achieve excellent results.

All available data is split into the categories *training*, *validation* and *test* data in a ratio of 80%/10%/10%. A batch-size of 32 is chosen for training. To increase the available data, the dataset is augmented by applying rotations, flipping and zooming onto the dataset. For each image size, the resulting dataset contains at least 1400 images. A rectifying linear (ReL) activation function is used for the convolution layers. A SoftMax activation function is used for the final layers.

5. Results

*5.1. General model accuracy: 450 px * 450 px*

To evaluate the model's performance during and after training, *model accuracy* and *model loss*, i.e. the percentage of correct and incorrect predictions during training are analyzed. These parameters are calculated after each training epoch and plotted in a graph. Since overfitting is a great concern, care is taken to



Fig. 4. Architecture of the regular CNN.

stop training accordingly, before overfitting occurs. Figure 5 shows accuracy and loss curves for all three models.

The basic CNN shows a steady increase in accuracy and decrease in loss up until the 25th epoch. Starting from the 26th epoch, training accuracy and loss stagnate or even reverse in trend. There is a significant increase in validation loss starting from the 26th epoch, indicating model overfitting. The final CNN model achieved a training accuracy of 0.8676 and a validation accuracy of 0.8828.

In comparison, accuracy and loss curves for the two pre-trained networks are analyzed and plotted. The first improvement to be noted is the greatly reduced number of epochs required to achieve final model training.

The VGG16 network starts to overfit from epoch 11 onwards. The learning curve shows a smoother course in general. After completed training, the VGG16 network shows a training accuracy of 0.9709 and a validation accuracy of 0.9500, greatly improving compared to the basic CNN.

Finally, the ResNet50 model shows similar results to the VGG16 model. It trains slightly faster than VGG16, showing

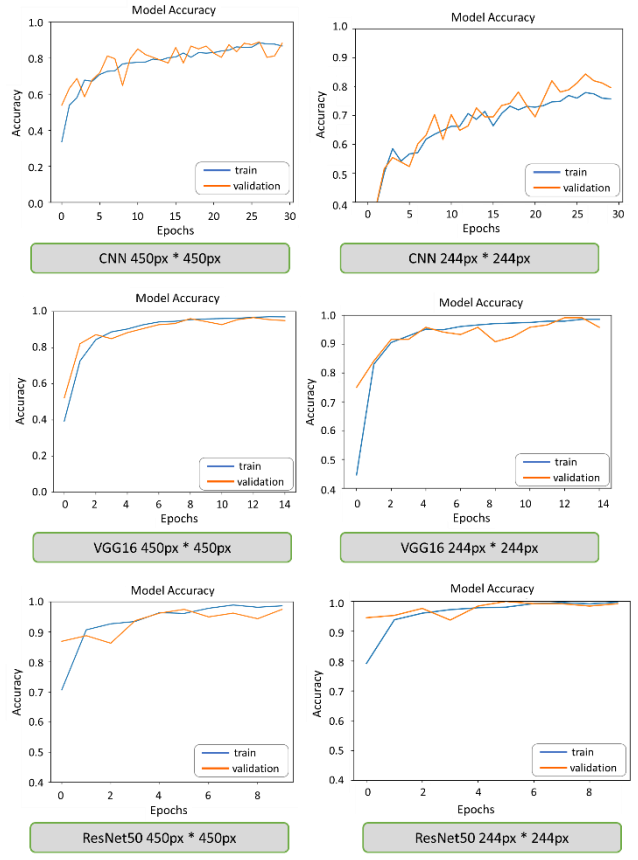


Fig. 5. Training and validation accuracies for all CNNs

excellent results from epoch 8 onwards. ResNet50 shows a slightly higher accuracy than VGG16, reaching a training accuracy of 0.9867 and a validation accuracy 0.9750. However, the learning curve is less smooth.

The results show the superiority of the pre-trained models, even for an industrial application with highly different images to their original training sample (i.e. ImageNet). It further indicates the necessity to create a vast dataset for truly precise classification of defects in LAFP. In total, the ResNet50 model shows the highest accuracy for the images with 450 px size. However, the validation accuracy lies slightly below the training accuracy, indicating that the model is slightly overfit.

Table 3. Training and validation accuracies of all considered CNNs (450px).

Network Model	Training Accuracy	Validation Accuracy
CNN	0.8676	0.8828
VGG16	0.9709	0.9500
ResNet50	0.9867	0.9750

*5.2. Analysis of defect classes: 450 px * 450 px*

Overall model accuracy is satisfactory with VGG16 and ResNet50. To generate a deeper understanding of the models' performance, the classification of each individual defect class is analyzed. For this purpose, a confusion matrix for every neural network is created, where true and false predictions can be seen according to their defect.

Figure 6 shows all three confusion matrices generated using the remaining test data. It is apparent that some defect classes are detected substantially more reliably. Additionally, each network exhibits different defect classes with which it struggles and which it detects reliably.

The regular CNN again shows the lowest performance. It fails to reliably detect most defects. The defect classes *tape rip* and *loose tape* show the highest detection rate with an accuracy of 0,95. The next best defect *thermal marks* is only detected with an accuracy of 0,7. The worst performance is seen with the *overlap* and the *gap* defect, where no accurate prediction is made. This is highly problematic, since those are the most commonly occurring defects during LAFP. Therefore, the CNN is not suitable for accurate defect prediction. It is interesting to note nonetheless that the CNN performs well in the *loose tape* defect, with which the other two networks show a weaker performance.

The VGG16 model shows an improved performance. All defect-free samples are predicted correctly. Predicting *thermal marks* and *tape rips* show an accuracy of 0,95. The next best prediction is the *gap* with 0,7. Gaps are often confused with tape rips, arguably because of their highly similar images. Finally, detecting an angular shift shows the poorest accuracy with 0,1. These defects are commonly seen as gaps, which can again be explained by their visual similarity. Reliable detection therefore requires more specialized algorithms. The ResNet50 model shows similar performance to VGG16. The *thermal marks* class shows the highest detection rate, being correctly detected each time. Close after, *tape rips* are detected with an

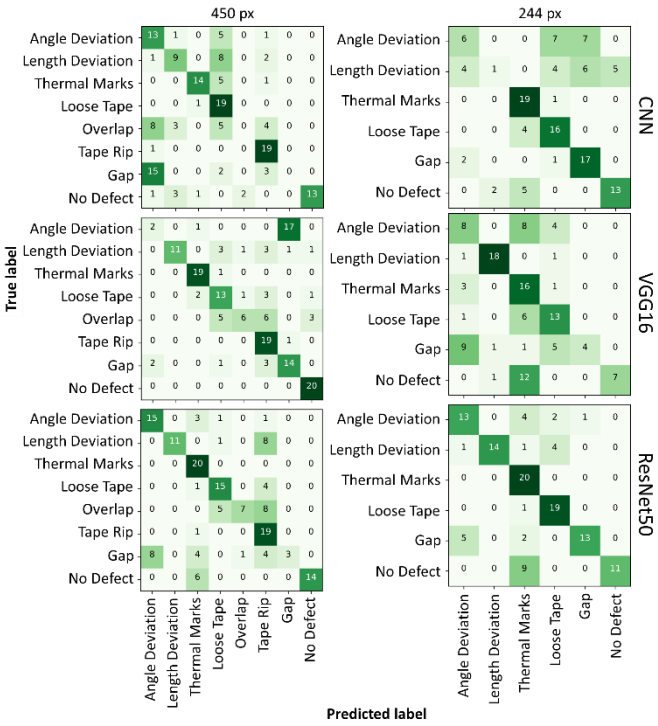


Fig. 6. Confusion matrices for CNNs, image size 450 px (l) and 244 px (r).

accuracy of 0,95. Interestingly, *angle deviations* are detected more reliably compared to VGG16. The ResNet50 struggles with *gaps*, confusing them with angle deviations and tape rips. *Overlaps* are here again detected poorly.

In general, the regular CNN underperforms compared to the pre-trained neural networks VGG16 and ResNet50. Furthermore, the *overlap* defect class cannot be reliably detected by any network. *Angle deviations* and *gaps* are often confused. Additionally, *tape rips* are sometimes confused for *gaps*. Therefore, the categories *tape rip* and *overlap* are omitted in the following.

*5.3. General model accuracy: 224 px * 224 px*

In a second approach, all three networks are trained on images of size 224 px * 224 px. Both VGG16 and ResNet50 have been pre-trained on images of this size in ImageNet.

When training the basic CNN, training and validation accuracy shows a very irregular course. The values start to stagnate around epoch 25 and decrease afterwards. The training accuracy lies under the validation accuracy and is relatively low. The maximum training accuracy lies at about 0,7868 while validation accuracy achieves 0,8594. These values are substantially lower compared to the 450 px CNN. Therefore, image size reduction for the classical CNN is not viable.

For VGG16, the accuracy increases with the smaller images. The training process is substantially faster, achieving a training optimum at epoch 12. A slight overfitting of the model can be seen thereon. Again, training is then stopped before this point is achieved. The model shows higher accuracy than the model trained on the larger images. The training accuracy achieves 0,9824 and the testing accuracy lies at 0,9833.

Lastly, the ResNet50 model shows similar results to the VGG16. The accuracy increases rapidly, excellent results are already achieved after 4 epochs. Slight overfitting can be seen starting from epoch 5 onwards. Training is stopped when training accuracy reaches 0,9991 and validation accuracy 1,0.

In general, the CNN model shows a lower performance when reducing pixel size. The pre-trained models show an increase in performance. Table 2 sums up all model accuracies.

Table 2. Training and validation accuracies of all considered CNNs (244px).

Network Model	Training Accuracy	Validation Accuracy
CNN	0,7868	0,8594
VGG16	0,9824	0,9833
ResNet50	0,9991	1,000

*5.4. Analysis of defect classes: 244 px * 244 px*

The regular CNN shows good accuracy for the defect classes *thermal marks*, *loose tape* and *gap* with values of respectively 0,95, 0,8 and 0,85. Defect-free placements are detected with a reliability of 0,65. However, the defect classes *angle deviation* and *length deviation* show poor detectability, being confused with almost every other defect class. The VGG16 model shows a higher mean performance over all defect classes. It detects length deviations with an accuracy of 0,9. Thermal marks show a detectability of 0,8. The VGG16 model struggles with the detection of gaps, only correctly detecting these in 20% of the cases. The ResNet50 model performs significantly better than the two previous models. Thermal marks are reliably detected each time. Loose tape defects show a similarly excellent detection rate with 0,95. In general, all remaining classes show a detection rate higher than 0,5. However, detecting defect-free tapes shows the lowest accuracy with 0,55.

6. Conclusions

This work presents an inline-capable defect detection setup for laser-assisted automated tape placement. An industrial camera system placed subsequent to the tape placement head is employed. The captured images are then fed to different types of CNNs for defect detection and classification. A bare CNN containing six convolution layers and six max-pooling layers is trained on the collected dataset. Additionally, two CNNs pre-trained on the ImageNet dataset (VGG16 and ResNet50) are adapted to the application using transfer learning.

All networks are trained on images of two sizes: 450 px * 450 px and 244 px * 244 px. Multiple commonly occurring defects are considered: *gaps, overlaps, loose tapes, tape rips, angle deviations, thermal degradation, length deviations.*

General training and validation accuracy of the trained CNNs are determined. The CNN without pre-training performs worst of all on images of size 244 px and second worst of all on images of size 450 px. This clearly shows that pre-training more complex networks even with unrelated images such as the

ImageNet dataset improves defect classification results substantially. The ResNet50 performs best of all with images of size 244 px, showing a validation accuracy of 1,0.

Performance on test data with which the network has not been trained reveals that all networks struggle with reliably predicting some defect classes. All CNNs are unable to predict overlaps, which led to the exclusion of this defect. VGG16 does not reliably predict angle deviations using 450 px images, confusing them with gaps. With 244 px, it struggles to predict gaps and angle deviations. On the opposite, the ResNet50 struggles to predict gaps with the 450 px images. For the 240 px images, gaps and angle deviations are predicted moderately well with a reliability of 0,65. ResNet50 with 244 px images gives the best compromise for defect detection.

In conclusion, the investigated method for defect detection shows limited applicability in an industrial environment as a stand-alone solution for general defect detection. Especially the poor detectability of overlap defects limits applicability of this method. For the other defects, a larger dataset in combination with more specific classification methods, e.g. using a combination of the employed CNNs with methods of classical computer vision and image processing could lead to improved results. Future work is required to investigate defect detectability on higher layers in the laminate.

Acknowledgements

Funded by the Deutsche Forschungsgemeinschaft (DFG, German Research Foundation) under Germany´s Excellence Strategy – EXC-2023 Internet of Production – 390621612.

References

[1] Heinecke, F., Willberg, C., 2019. Manufacturing-Induced Imperfections in Composite Parts Manufactured via Automated Fiber Placement 3, p. 56.
[2] Gholizadeh, S., 2016. A review of non-destructive testing methods of composite materials 1, p. 50.
[3] Marrouzé, J., Housner, J., Abdi, F., 2013. Effect of manufacturing defects and their uncertainties on strength and stability of stiffened panels, in 19th International Conference on Composite Materials, Montreal, Canada, p. 7596.
[4] Li, X., Hallett, S.R., Wisnom, M.R., 2015. Modelling the effect of gaps and overlaps in automated fibre placement (AFP)-manufactured laminates 22, p. 115.
[5] Nguyen, M.H., Davidson, P., Waas, A.M., 2021. Experimental and numerical study on the tensile failure behavior of toughened-interlayer composite laminates with automated fiber placement (AFP) induced gap and overlap defects 14, p. 105.
[6] Nguyen, M.H., Vijayachandran, A.A., Davidson, P., Call, D. et al., 2019. Effect of automated fiber placement (AFP) manufacturing signature on mechanical performance of composite structures 228, p. 111335.
[7] Sawicki, A., Minguett, P., 1998. The effect of intraply overlaps and gaps upon the compression strength of composite laminates, in 39th AIAA/ASME/ASCE/AHS/ASC Structures, Structural Dynamics, and Materials Conference and Exhibit, American Institute of Aeronautics and Astronautics, Reston, Virigina.
[8] Shadmehri, F., Ioachim, O., Pahud, O., Brunel, J.-E. et al., 2015. Laser-vision inspection system for automated fiber placement (AFP) process, in 20th International Conference on Composite Materials.
[9] Rudberg, T., Cemenska, J., 2012. Incorporation of Laser Projectors in Machine Cell Controller Reduces Ply Boundary Inspection Time, On-Part Course Identification and Part Probing 5, p. 74.
[10] Cemenska, J., Rudberg, T., Henscheid, M., 2015. Automated In-Process Inspection System for AFP Machines 8, p. 303.
[11] Schuster, A., Mayer, M., Willmeroth, M., Brandt, L. et al., 2020. Inline Quality Control for Thermoplastic Automated Fibre Placement 51, p. 505.
[12] Sacco, C., Baz Radwan, A., Anderson, A., Harik, R. et al., 2020. Machine learning in composites manufacturing: A case study of Automated Fiber Placement inspection 250, p. 112514.
[13] Sacco, C., Radwan, A.B., Anderson, A., Harik, R., 2020. NDE Inspection of AFP Manufactured Cylinders Using an Intelligent Segmentation Algorithm, in SAMPE 2020 Conference and Exhibition.
[14] Sacco, C., Radwan, A.B., Beatty, T., Harik, R., 2019. Machine learning based AFP inspection: A tool for characterization and integration, in SAMPE 2019 Conference and Exhibition.
[15] Saeed, N., King, N., Said, Z., Omar, M.A., 2019. Automatic defects detection in CFRP thermograms, using convolutional neural networks and transfer learning 102, p. 103048.
[16] Kuhl, M., Wiener, T., Krauß, M., 2013. Multisensorial Self-learning Systems for Quality Monitoring of Carbon Fiber Composites in Aircraft Production 12, p. 103.
[17] Meister, S., Wermes, M., Stüve, J., Groves, R.M., 2021. Cross-evaluation of a parallel operating SVM – CNN classifier for reliable internal decision-making processes in composite inspection 60, p. 620.
[18] Yoon, S., Kim, A., Cantwell, W.J., Yeun, C.Y. et al., 2023. Defect detection in composites by deep learning using solitary waves 239, p. 107882.
[19] Tang, Y., Wang, Q., Wang, H., Li, J. et al., 2021. A novel 3D laser scanning defect detection and measurement approach for automated fibre placement 32, p. 75201.
[20] Tang, Y., Wang, Q., Cheng, L., Li, J. et al., 2022. An in-process inspection method integrating deep learning and classical algorithm for automated fiber placement 300, p. 116051.
[21] Tao, Y., Jia, S., Duan, Y., Zhang, X., 2016. An online detection method for composite fibre tow placement accuracy 230, p. 1614.
[22] Brysch, M., Bahar, M., Hohensee, H.C., Sinapius, M., 2022. Single system for online monitoring and inspection of automated fiber placement with object segmentation by artificial neural networks 33, p. 2013.
[23] Zhang, Y., Wang, W., Liu, Q., Guo, Z. et al., 2022. Research on Defect Detection in Automated Fiber Placement Processes Based on a Multi-Scale Detector 11, p. 3757.
[24] Meister, S., Wermes, M.A.M., Stüve, J., Groves, R.M., 2021. Review of image segmentation techniques for layup defect detection in the Automated Fiber Placement process 32, p. 2099.
[25] Meister, S., Wermes, M.A.M., Stueve, J., Groves, R.M., 2020 - 2020. Algorithm assessment for layup defect segmentation from laser line scan sensor based image data, in Sensors and Smart Structures Technologies for Civil, Mechanical, and Aerospace Systems 2020, SPIE, p. 45.
[26] Meister, S., Wermes, M., 2022. Performance evaluation of CNN and R-CNN based line by line analysis algorithms for fibre placement defect classification.
[27] Meister, S., Wermes, M., Stüve, J., Groves, R.M., 2021. Investigations on Explainable Artificial Intelligence methods for the deep learning classification of fibre layup defect in the automated composite manufacturing 224, p. 109160.
[28] Meister, S., Wermes, M.A.M., Stüve, J., Groves, R.M., 2021 - 2021. Explainability of deep learning classifier decisions for optical detection of manufacturing defects in the automated fiber placement process, in Automated Visual Inspection and Machine Vision IV, SPIE, p. 3.
[29] Meister, S., Möller, N., Stüve, J., Groves, R.M., 2021. Synthetic image data augmentation for fibre layup inspection processes: Techniques to enhance the data set 32, p. 1767.
[30] Emonts, M., Fischer, K., Peitz, A., Weiler, T., 2020. Ultra-fast Consolidator Machine Development – Individualized Mass Production of Thermoplastic Tailored Blanks based on Laser-assisted Tape Placement with in-situ Consolidation *3*